ADVANCED FUNCTIONAL MATERIALS
www.afm-journal.de

www.MaterialsViews.com

Inserting Sn Nanoparticles into the Pores of TiO_{2-x}–C Nanofibers by Lithiation

Xiaoyan Li, Yuming Chen, Hongtao Wang, Haimin Yao, Haitao Huang, Yiu-Wing Mai, Ning Hu, and Limin Zhou**

Tin holds promise as an anode material for lithium-ion batteries (LIBs) because of its high theoretical capacity, but its cycle life is limited by structural degradation. Herein, a novel approach is exploited to insert Sn nanoparticles into the pores of highly stable titanium dioxide–carbon (TiO_{2-x}–C) nanofiber substrates that can effectively localize the postformed smaller Sn nanoparticles, thereby address the problem of structural degradation, and thus achieve improved anode performance. During first lithiation, a $Li_{4.4}Sn$ alloy is inserted into the pores surrounding the initial Sn nanoparticles in TiO_{2-x}–C nanofibers by its large volume expansion. Thereafter, the original Sn nanoparticle with a diameter of about 150 nm cannot be recovered by the delithiation because of the surface absorption between inserted Sn nanoparticles and the TiO_{2-x}–C substrate, resulting in many smaller Sn nanoparticles remaining in the pores. Batteries containing these porous TiO_{2-x}–C–Sn nanofibers exhibit a high capacity of 957 mAh g^{-1} after 200 cycles at 0.1 A g^{-1} and can cycle over 10 000 times at 3 A g^{-1} while retaining 82.3% of their capacity, which represents the longest cycling life of Sn-based anodes for LIBs so far. This interesting method can provide new avenues for other high-capacity anode material systems that suffer from significant volume expansion.

1. Introduction

Rechargeable lithium-ion batteries (LIBs) are regarded as a promising power source for electronic devices such as electric vehicles and hybrid electric vehicles.[1–5] Graphite, as the most intensely used commercial anode material, has a low theoretical capacity of 372 mAh g^{-1}, which makes it difficult to meet the demands for high energy density in energy storage systems. Recently, Sn has been widely studied as an anode material for LIBs due to its high theoretical capacity of 991 mAh g^{-1}. However, the rapid fading of capacity that results from the great change in volume during the alloying-dealloying reaction between Sn and Li renders the achievement of a long cycle life difficult.[6–12] Recent years, great efforts have been devoted to solve the above issues by a) engineering nanostructure to reduce the volume expansion; b) incorporating Sn with other phases, including carbon and titanium dioxide, not only to prevent the aggregation of Sn but serve as buffer scaffold.[13–23] Nevertheless, long-term cycling performance of the existing Sn-based anode remains unsatisfactory. To obtain desirable cycling performance, our objective is to scrupulously design a robust porous 1D TiO_{2-x}–carbon (TiO_{2-x}–C) substrate to encapsulate Sn nanoparticles, in which the firm TiO_{2-x}–C substrate can fully absorb the volume expansion of the Sn nanoparticles in the TiO_{2-x}–C substrate during charging-discharging processes (which can be directly observed by in situ transmission electron microscopy [TEM]) and thus achieve a long life.

Dr. X. Y. Li, Dr. Y. M. Chen, Prof. H. M. Yao, Prof. Y.-W. Mai, Prof. L. M. Zhou
Department of Mechanical Engineering
The Hong Kong Polytechnic University
Hong Kong, China
E-mail: yumingc126@126.com; mmlmzhou@polyu.edu.hk
Prof. H. T. Wang
Institute of Applied Mechanics
Zhejiang University
Hangzhou 310027, China
Prof. H. T. Huang
Department of Applied Physics and Materials Research Center
The Hong Kong Polytechnic University
Hong Kong, China
Prof. Y.-W. Mai
Centre for Advanced Materials Technology (CAMT)
School of Aerospace
Mechanical and Mechatronics Engineering J07
The University of Sydney
NSW 2006, Australia
Prof. N. Hu
College of Aerospace Engineering
Chongqing University
Chongqing 401331, China

DOI: 10.1002/adfm.201503711

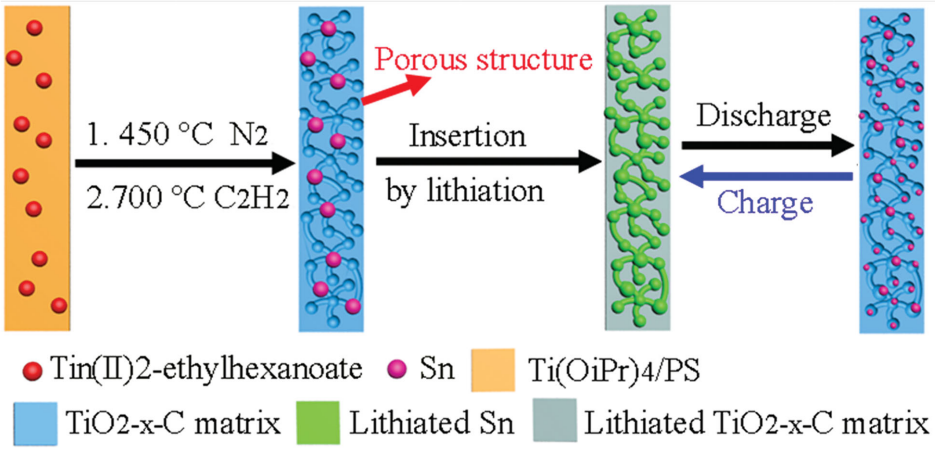

Figure 1. Schematic illustration of the formation of highly stable porous TiO_{2-x}–C–Sn composite nanofibers and insertion of Sn nanoparticles.

In this study, for the first time, we present a novel approach of lithiation-induced insertion of Sn nanoparticles into the pores of the highly stable TiO_{2-x}–C nanofiber substrates, which can effectively localize the Sn nanoparticles and allow superior performance. In situ TEM was performed to characterize the structural evolution of the prepared material during the charging and discharging processes. It was found that $Li_{4.4}Sn$ alloy was inserted into the pores surrounding the initial Sn nanoparticles in the TiO_{2-x}–C nanofibers by its large volume expansion. The initial Sn nanoparticle with diameter of about 150 nm could not be recovered after discharging due to the surface absorption between smaller separated Sn nanoparticles and TiO_{2-x}–C substrate. These detached Sn nanoparticles remained in the pores which are able to accommodate their expansions, thus yielding a very long cycle life.

2. Results and Discussion

2.1. Synthesis and Characterization of Highly Stable Porous TiO_{2-x}–C–Sn Composite Nanofibers

The detailed fabrication process is shown in **Figure 1**. First, the $Ti(OiPr)_4$–polystyrene–tin(II)2-ethylhexanoate fibers were synthesized through electrospinning. The electrospun $Ti(OiPr)_4$–polystyrene–tin(II)2-ethylhexanoate fibers were treated at 450 °C in an atmosphere of N_2 to obtain porous TiO_2–C–SnO_x, in which part of the polystyrene turned into carbon and others were burnt out to form pores, followed by treatment in a mixture of C_2H_2/H_2/Ar at 700 °C to achieve porous TiO_{2-x}–C–Sn composite nanofibers. Some parts of the Ti^{4+} were reduced to Ti^{3+} by heating in a hydrogen atmosphere, which resulted in the presence of oxygen vacancies and Ti^{3+} species and thus effectively improved the electrical conductivity of TiO_2.[24–26]

The FESEM and TEM images in **Figure 2**a,b reveal the fibrous morphology of the resulting materials, with a highly porous surface of nanofibers with diameters of 400 to 500 nm. These surface pores facilitate rapid access of the lithium ions into the inner fibers, yielding a good rate capability and activation of all of the materials. It is clear that the Sn nanoparticles are encapsulated in the porous TiO_{2-x}–C composite substrate as shown in Figure 2c,d. A magnified image in Figure 2e exhibits the highly porous inner structure, which is beneficial for accommodation of the variation in the volume of Sn during repeated charging and discharging cycles. The prepared TiO_{2-x}–C–Sn hybrid shows a relatively high Brunauer–Emmett–Teller specific area of 83.1 $m^2\ g^{-1}$ with a pore volume of 0.285 $cm^3\ g^{-1}$. As shown in Figure S1a of the Supporting Information, the pore size distribution curve calculated by a nonlocal density functional theory method indicates that the prepared hybrid involves nanopores ranging in size from 1.5 to 68 nm. Figure S1b of the Supporting Information shows the isothermal plot of the porous TiO_{2-x}–C–Sn composite nanofibers, which is characteristic of the porous structure.[27] The high-resolution TEM image in Figure 2f confirms the presence of tetragonal Sn ($d_{Sn(200)}$ = 0.29 nm), rutile TiO_2 ($d_{TiO2\ (101)}$ = 0.24 nm), and carbon, which is consistent with the results of selected area electron diffraction (SAED, Figure 2d), XRD (**Figure 3**a), and Raman analysis (Figure S2, Supporting Information).[9,28]

The surface chemistry of the porous TiO_{2-x}–C–Sn composite nanofibers was analyzed by XPS. The typical XPS spectrum of TiO_{2-x}–C–Sn nanofibers in Figure S3a of the Supporting Information demonstrates the existence of C, Ti, Sn, and O, which is in good agreement with the result of EDS in Figure S4 and the elemental line scanning in Figure S5 of the Supporting Information. As shown in Figure 3b, the Sn 3d spectrum displays two typical peaks at 487.2 and 495.7 eV, assigning to Sn $3d_{5/2}$ and Sn $3d_{3/2}$, which shows that some Sn nanoparticles near the surface of the fiber have been oxidized into SnO_2.[14,29,30] Peak separation of the Ti 2P spectrum in Figure 3c presents four peaks with binding energies of 458, 463.5, 458.7, and 464.5 eV, respectively. The peaks at 458 and 463.5 eV are attributed to Ti^{3+}, and the bands at 458.7 and 464.5 eV are attributed to Ti^{4+}.[31,32] The composition distribution in Table S1 of the Supporting Information demonstrates the existence of non-stoichiometric titanium suboxides. The high-resolution XPS spectrum of C 1s (Figure 3d) can be deconvoluted into three peaks. The peak at 284.5 eV is assigned to the C–C bonds, and the other two peaks at 285.8 and 288 eV correspond to the C–O and C=O bonds, which would be due to the partial

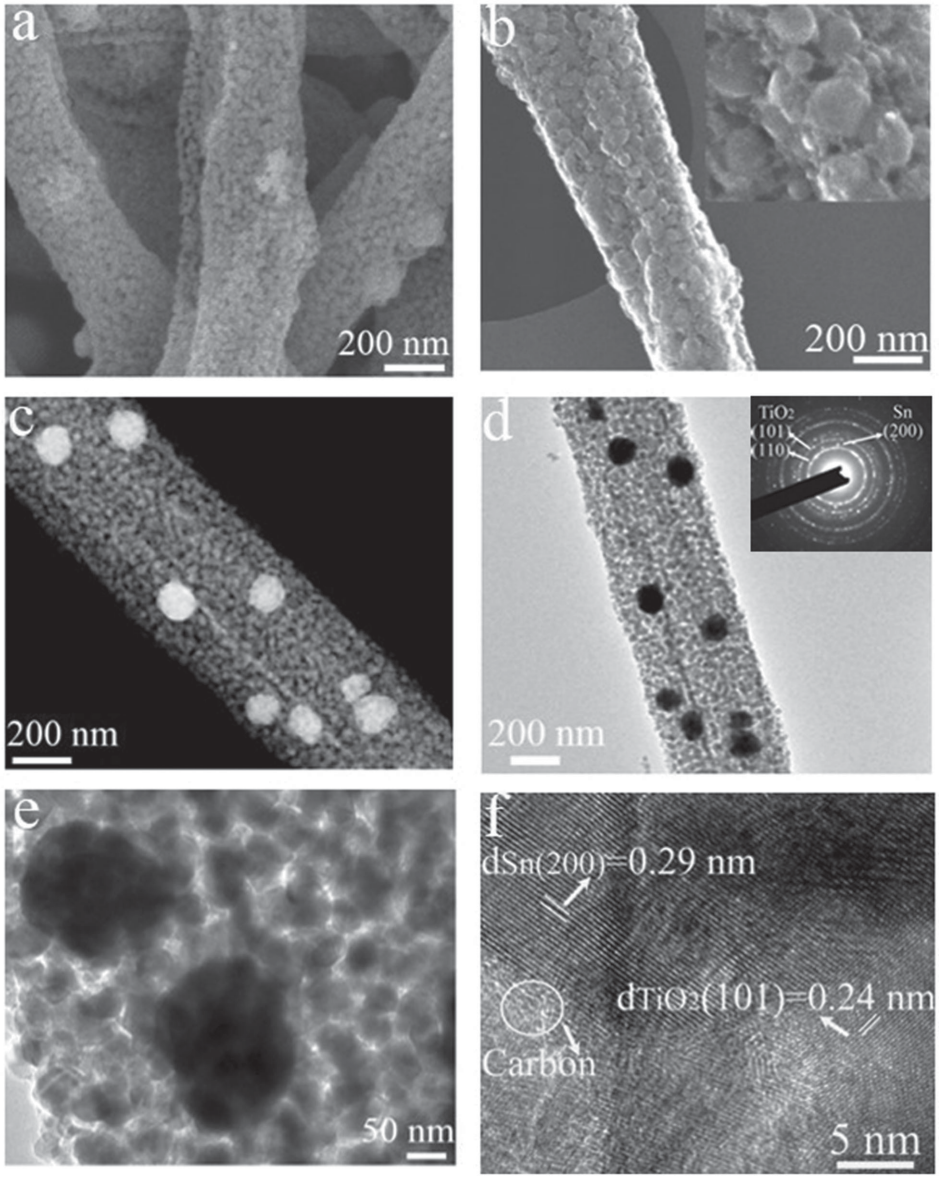

Figure 2. Morphology of the highly stable porous TiO_{2-x}–C–Sn composite nanofibers. a) FESEM, b) TEM-SEI, c) TEM-BF, d,e) TEM, and f) HRTEM images of TiO_{2-x}–C–Sn nanofibers. The inset in (d) is a SAED pattern.

substitution of some of lattice titanium atoms by carbons and the organic carbonacous material resulting from the calcination of oxygen-containing organic precursors such as tin(II)2-ethylhexanoate, respectively.[16,32–35] In Figure S3b of the Supporting Information, the O 1s spectrum is divided into three peaks at 530 eV (Ti—O), 531 eV (H—O), and 532.5 eV (C—O).[16]

2.2. Morphology Evaluation of the TiO_{2-x}–C–Sn Composite Nanofibers upon Cycling

In situ TEM was used to observe the structural evolution of the prepared material during the processes of charging and discharging. **Figure 4** shows the typical morphological evolution of Sn nanoparticles encapsulated in the porous TiO_{2-x}–C nanofiber during the first five charging and discharging processes. Obvious volume expansion occurred after the first lithiation, as shown in Figure 4a. Apparently, the pores surrounding the Sn nanoparticles in the composite nanofiber were able to absorb the expansion of the Sn nanoparticles without inducing a change in the volume of the TiO_{2-x}–C composite nanofiber substrate, proving the firmness and excellent mechanical properties of TiO_{2-x}–C matrix. The uniform dark contrast of Sn nanoparticles became lighter with the reaction processing. The Sn nanoparticles underwent a volume change of approximately 260% at the completion of the first charging process. The lithium was gradually extracted from the Li–Sn alloys when the process of delithiation began, as displayed in

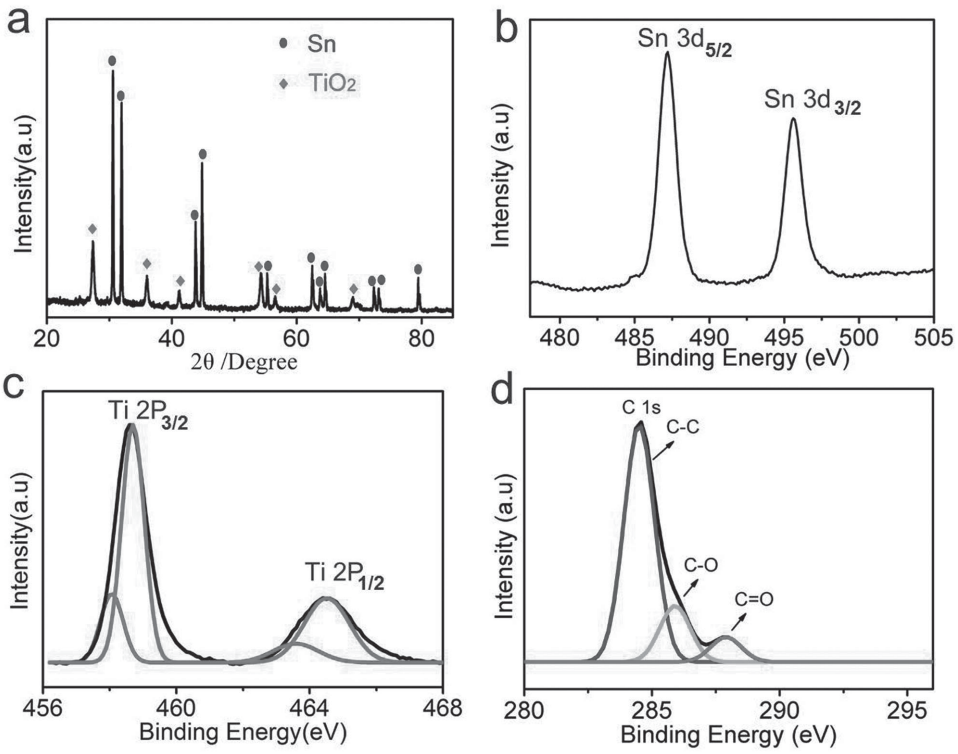

Figure 3. Characterization of highly stable porous TiO_{2-x}–C–Sn composite nanofibers. a) Typical XRD pattern, b–d) XPS of spectra of the porous TiO_{2-x}–C–Sn composite nanofibers: b) Sn 3d, c) Ti 2p, and d) C 1s spectrum.

Figure 4b. The Sn nanoparticles separated into smaller particles after the first discharging process due to the surface absorption force between Sn nanoparticle and TiO_{2-x}–C substrate.[36] The separated Sn nanoparticles did not recover their original volume after the second lithiation (Figure 4c). The smaller Sn nanoparticles remained in the pores toward which the initial Sn nanoparticles expanded. These pores were able to accommodate the expansion of the separated Sn nanoparticles with diameter ranging from 2 to 30 nm, which can be shown by the lack of a clear change in Figure 4d as compared with Figure 4c.

Ex situ TEM was also used to observe the structural changes in the porous TiO_{2-x}–C–Sn nanofibers after different charge–discharge cycles (**Figure 5**). The Sn nanoparticles, which occupy the pores that surround them, are unable to convert back to their original state after the first charge–discharge cycle. The enlarged figure inset in Figure 5a and line scanning in Figure 5b confirm the detachment of the Sn nanoparticles into smaller particles. Obviously, the size of the Sn nanoparticles decreased greatly as induced by lithiation after 1000 cycles, as shown in Figure 5c. The line scanning in Figure 5d demonstrates the uniform distribution of the smaller Sn nanoparticles in the porous TiO_{2-x}–C substrate, facilitating the transport of electrons, which can be proven by the electrochemical impedance spectroscopy shown in Figure S6 of the Supporting Information. The high-resolution TEM images in the insets of Figure 5a,c clearly demonstrates that the crystalline structure of Sn and TiO_2 does not change after cycling. In addition, no loss of Sn can be found, which demonstrates great stability.

2.3. Electrochemical Performance

The electrochemical performance of the TiO_{2-x}–C–Sn electrode is evaluated in **Figure 6**. Figure 6a depicts the charge–discharge voltage profiles of the TiO_{2-x}–C–Sn nanofibers at a current density of 0.1 A g^{-1}. The discharge and charge capacities are 1562 and 1045 mAh g^{-1}, respectively, displaying a Coulombic efficiency of 67%. The loss of capacity can be ascribed to the formation of an solid electrolyte interface layer and the decomposition of electrolytes.[9,13,14,37,38] It is worth noting that the correlative plateaus are in good agreement with the cyclic voltammetry results in Figure S7 of the Supporting Information.[6,10,39,40] Figure 6b compares the cycling performance of three electrodes made of TiO_{2-x}–C–Sn, TiO_2–C, and TiO_2 nanofibers at a current density of 0.1 A g^{-1} between 0 and 3 V. The capacity of TiO_{2-x}–C–Sn nanofibers decreases during the first few cycles and then gradually rises, finally reaching and maintaining 957 mAh g^{-1} after 200 cycles. The increase in capacity is mainly a result of the material activation after cycling. In comparison, the TiO_2–C and TiO_2 electrodes can only deliver capacities of 422 and 122 mAh g^{-1} at 0.1 A g^{-1}, respectively. The TiO_{2-x}–C–Sn electrode was assessed by charging and discharging at different rates from 0.5 to 5 A g^{-1}, as shown in Figure 6c. It maintains high reversible capacities of 374, 336, 275, 204, and 133 mAh g^{-1} at 0.5, 1, 2, 3, and 5 A g^{-1}, respectively, and the capacity of 275 mAh g^{-1} can be attained again when the current density returns to 2 A g^{-1}. Most importantly, the battery can cycle over 10 000 times with a remained capacity of 140 mAh g^{-1} at 3 A g^{-1} (Figure 6c), which kept more than 82.3% of their capacity

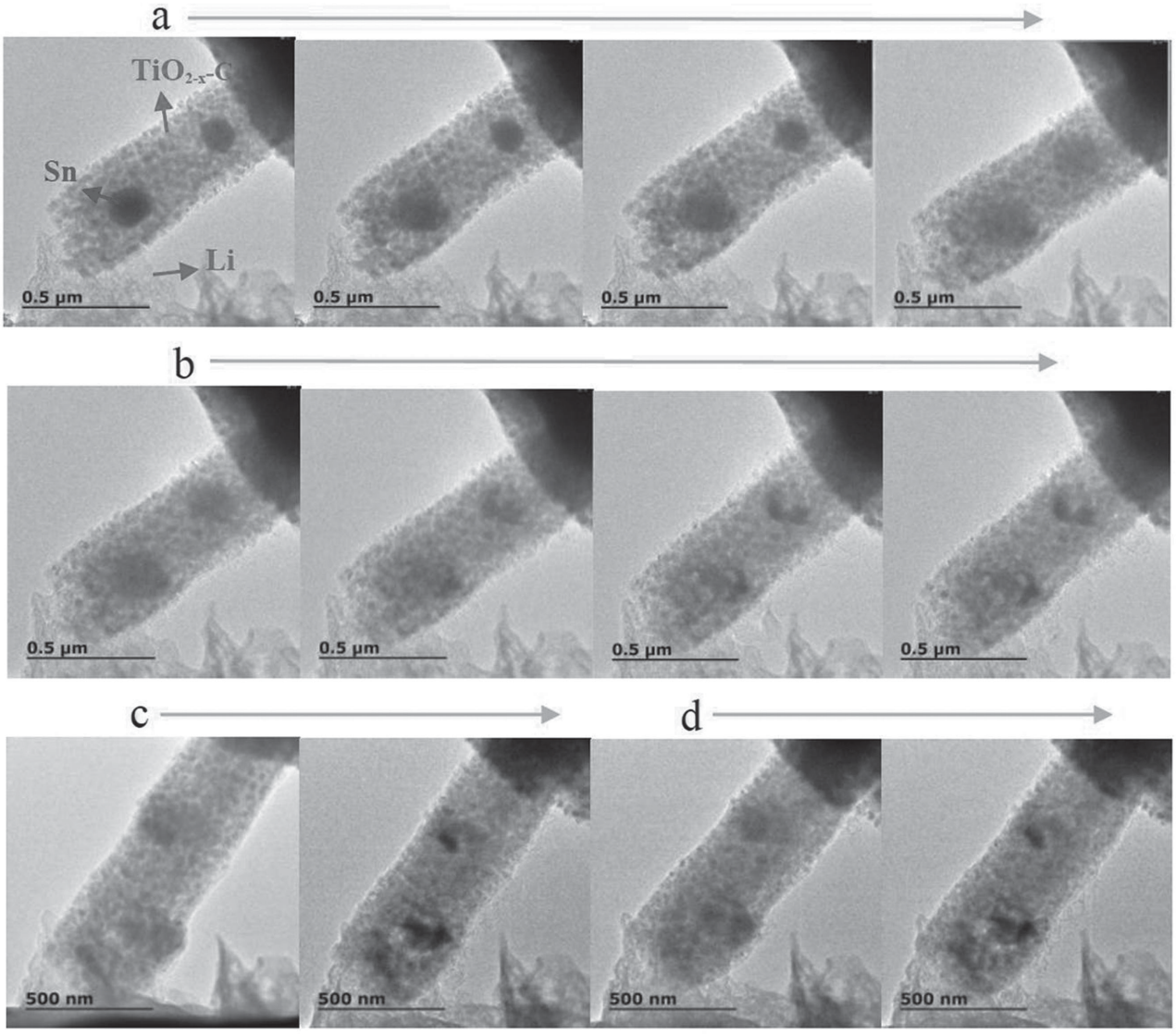

Figure 4. Typical morphological evolutions of Sn nanoparticles in the highly stable porous TiO_{2-x}–C nanofiber. a) The first charging process, b) the first discharging process, c) the second charging/discharging steps, and d) the fifth charging/discharging steps.

(0.177% decay per 100 cycles), showing a very long cycling life. While the capacity of TiO_2 only remains at 40 mAh g^{-1} at 3 A g^{-1}, as shown in Figure S8 of the Supporting Information. To the best of our knowledge, this is the longest cycling life of Sn-based anodes which has not discovered before. Figure S9 of the Supporting Information shows the charge–discharge profiles after 200 cycles and at different current densities. It is clear that the plateaus of Sn lithiation and delithiation can be obviously observed after 200 cycles (Figure S9a, Supporting Information), indicating that the Sn nanomaterials are still well maintained in the TiO_{2-x}–C composite substrate. Furthermore, the contributions of different components to the whole capacity can also be seen through these charge–discharge profiles. The measurement on electrochemical performance of the hybrid materials in the voltage range of 0–1 V has been also conducted (Figure S10, Supporting Information). Figure S10a of the Supporting Information shows that the porous TiO_{2-x}–C–Sn nanofibers have the reversible capacity of ≈443 mAh g^{-1} after 10 cycles at 0.1 A g^{-1} based on the mass of the whole composite. If based on the mass of Sn (48.12 wt% of Sn in the composite, Table S1, Supporting Information), the reversible capacity can be up to 920 mAh g^{-1}, which is close to the theoretical capacity of Sn. Moreover, this hybrid material still has high capacities of ≈622, 538, 500, 408 and 311 mAh g^{-1} at current densities of 0.4, 0.6, 0.8, 1, and 2 A g^{-1}, respectively, based on the mass of Sn. These results show that our material possesses high electrochemical performance. For the practical application, the low Coulombic efficiency for the composite in the initial cycle would be addressed by creating a passivation layer on the surface of the prepared anode.[3] The superior electrochemical performance of the TiO_{2-x}–C–Sn nanofibers may be attributable to the following benefits. i) The high theoretical capacity of Sn contributes to the capacity of the nanofiber substrate. ii) The TiO_{2-x} nanofiber substrate leads to structural stability and thus to good cyclability.

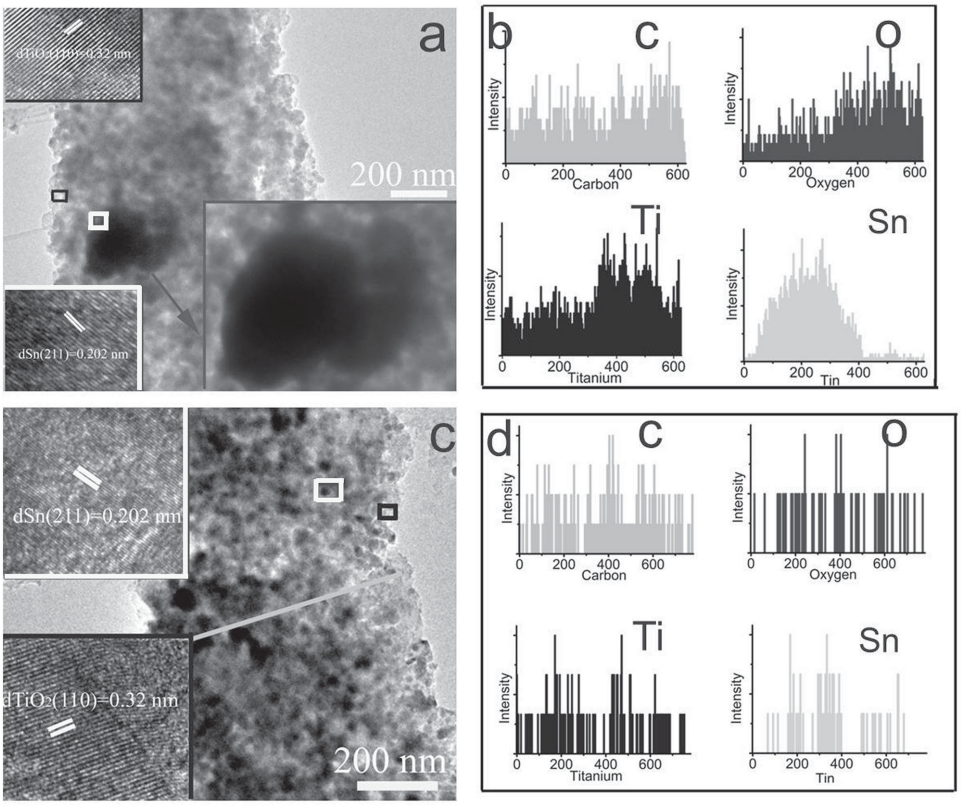

Figure 5. TEM and HRTEM images of the highly stable porous TiO_{2-x}–C–Sn composite nanofiber electrode after a) 1 and c) 1000 charge–discharge cycles, b,d) corresponding line scanning of (a,c), respectively.

iii) The porous structure provides void space to accommodate the changes in volume of Sn nanoparticles during the charging and discharging cycles, which is beneficial for maintaining the integrity of the material and further enhancing the cycle life. iv) 1D nanostructure and carbon facilitate the rapid transport of ion and electrons and yield an excellent rate capability.[41,42] v) Ti^{3+}-doped TiO_{2-x} results in a significant increase in electronic conductivity, which benefits electrochemical lithium storage.

3. Conclusions

In summary, we exploited a novel approach of lithiation-induced insertion of Sn nanoparticles into the pores of highly stable TiO_{2-x}–C nanofiber substrates to address the problem of structural degradation of Sn-based electrode. The in situ TEM observation has proved that during first lithiation $Li_{4.4}Sn$ alloy can be effectively inserted into the pores surrounding the initial Sn nanoparticles in the TiO_{2-x}–C nanofibers by its large volume expansion and after first delithiation the post-formed smaller Sn nanoparticles remain in the pores. Benefiting from the unique structural and compositional features, the as-made TiO_{2-x}–C–Sn nanofibers as anode have achieved a long cycling life of over 10 000 charging–discharging cycles in addition to a high specific capacity of 957 mAh g^{-1} at 0.1 A g^{-1} and good rate capability. We believe that this novel and simple approach could provide new avenues for synthesizing other high-performance anode material systems that suffer from large volume expansion.

4. Experimental Section

Synthesis of 1D Porous TiO_{2-x}–C–Sn Composite Nanofibers: A 3 g sample of polystyrene ($M_W \approx 280\,000$) was dissolved in 20 mL of dimethylformamide at 70 °C for 5 h with vigorous stirring. Then, 1 mL of acetic acid and 3 mL of $Ti(OiPr)_4$ were added dropwise into the polystyrene solution, followed by 1 mL of tin(II)2-ethylhexanoate. The precursor solution was used for electrospinning at a high voltage of 17 kV. The distance between the needle and the drum collector was fixed at 20 cm, and the feeding rate was set at 0.04 mm min^{-1} (KATO Tech Co., Ltd). The collected films were first heated at 450 °C in an atmosphere of N_2 and then treated in a C_2H_2/H_2/Ar mixture at 700 °C for 30 min to prepare porous TiO_{2-x}–C–Sn composite nanofibers.

Characterization: The morphologic features of the samples were examined by field emission scanning electron microscopy (FESEM, JEOL 6300F), TEM, and high-resolution TEM (JEOL 2100F). A JEOL 2100 TEM equipped with a Nanofactory STM-TEM holder was used to conduct the in situ electrochemical experiments. The crystal structure was examined by X-ray diffraction (XRD, Philips X'Pert Pro MPD). Measurement by X-ray photoelectron spectroscopy (XPS) was performed on a Perkin-Elmer model PHI 5600 system with a monochromated aluminum anode X-ray source. A Micromeritics ASAP2020 analyzer was used to evaluate the surface area.

Electrochemical Test: The electrochemical performance of the TiO_{2-x}–C–Sn composite nanofiber electrode was measured using CR 2032 coin cells that were assembled in an Ar-filled glove box. The working electrode was

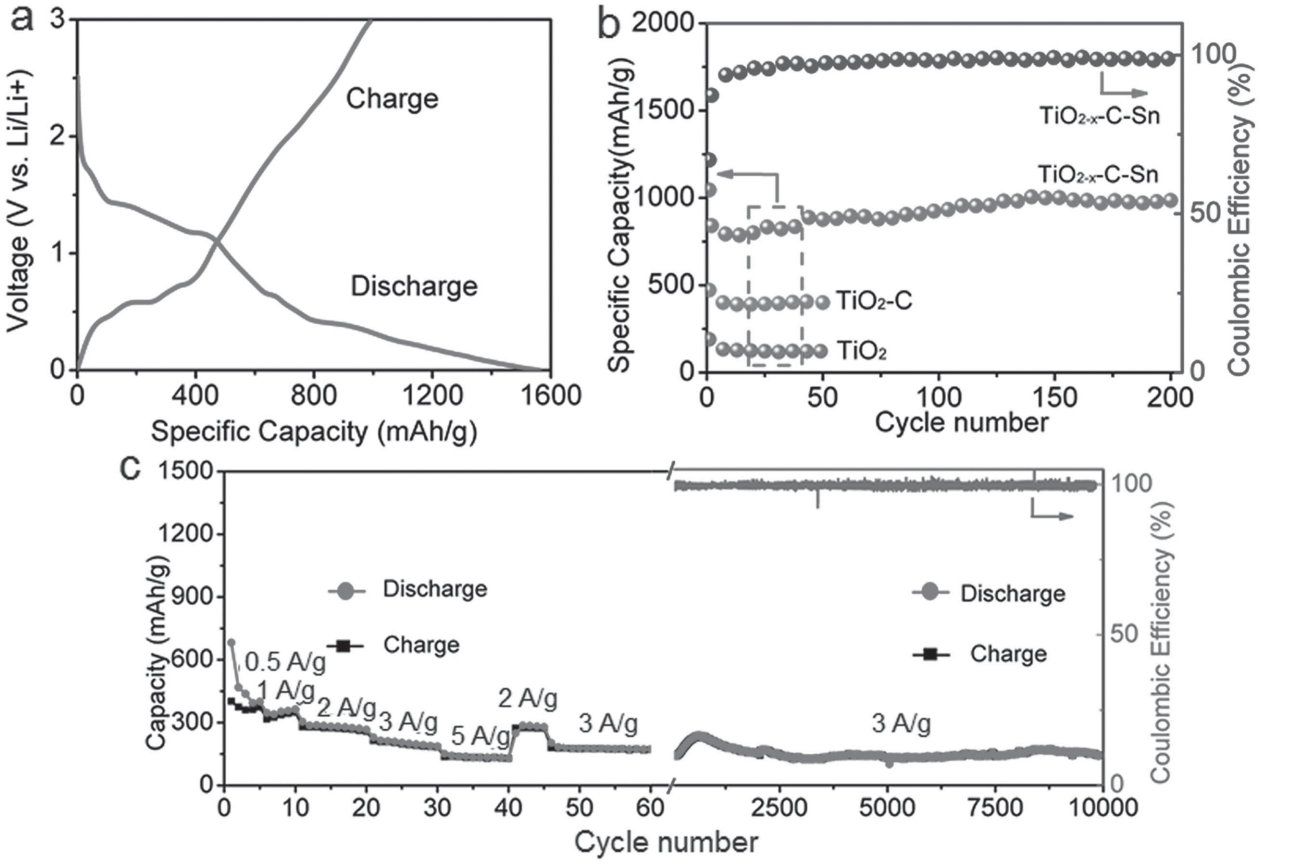

Figure 6. Electrochemical performance of the highly stable porous TiO_{2-x}–C–Sn composite nanofiber electrodes. a) Charge–discharge profile, b) cycling performance of TiO_{2-x}–C–Sn, TiO_2–C, and TiO_2 nanofibers at the rate of 0.1 A g^{-1}, c) rate and cycling performance of the porous TiO_{2-x}–C–Sn composite nanofibers.

made of the active materials, carbon black, and polyvintlidene fluoride binder slurry in a weight ratio of 8:1:1, which was coated on the copper foil current collector. Metallic lithium was used as the counter electrode, and celgard 2400 film was used as the separator. The electrolyte solution was 1 M of $LiPF_6$ in a mixture of ethylene carbonate/diethyl carbonate (1:1 v/v). The charge and discharge tests were carried out in the range of 0 to 3 V with a battery testing system (LAND 2001 CT). Cyclic voltammetry was performed on a CHI 660C electrochemical workstation between 0 and 3 V at a scan rate of 0.1 mV s^{-1}.

Supporting Information

Supporting Information is available from the Wiley Online Library or from the author.

Acknowledgements

The authors are grateful for the support received from the Research Grants Council of the Hong Kong Special Administration Region (Grant No. PolyU5312/12E) and the Hong Kong Polytechnic University (Grant Nos. G-YBA1, G-YBDG, and 1-BBZN).

Received: September 2, 2015
Revised: October 6, 2015
Published online: December 7, 2015

[1] Y. Guo, L. Yu, C. Y. Wang, Z. Lin, X. W. Lou, *Adv. Funct. Mater.* **2015**, *25*, 5184.
[2] B. Zhang, J. Q. Huang, J. K. Kim, *Adv. Funct. Mater.* **2015**, *25*, 5222.
[3] Y. M. Chen, X. Y. Li, K. Park, J. Song, J. H. Hong, L. M. Zhou, Y. W. Mai, H. T. Huang, J. B. Goodenough, *J. Am. Chem. Soc.* **2013**, *135*, 16280.
[4] H. Hu, L. Yu, X. H. Gao, Z. Lin, X. W. Lou, *Energy Environ. Sci.* **2015**, *8*, 1480.
[5] L. Zhang, H. B. Wu, B. Liu, X. W. Lou, *Energy Environ. Sci.* **2014**, *7*, 1013.
[6] W. M. Zhang, J. S Hu, Y. G. Guo, S. F. Zheng, L. S. Zhong, W. G. Song, L. J. Wan, *Adv. Mater.* **2008**, *20*, 1160.
[7] Y. Yu, G. Lin, C. L. Wang, A. Dhanabalan, P. A. V. Aken, J. Maier, *Angew. Chem. Int. Ed.* **2009**, *48*, 6485.
[8] Y. H. Xu, Q. Liu, Y. J. Zhu, Y. H. Liu, A. Langrock, M. R. Zachariah, C. S. Wang, *Nano Lett.* **2013**, *13*, 470.
[9] Y. Q. Zou, Y. Wang, *ACS Nano* **2011**, *5*, 8108.
[10] Y. Yu, L. Gu, C. B. Zhu, P. A. V. Aken, J. Maier, *J. Am. Chem. Soc.* **2009**, *131*, 15984.
[11] Z. Q. Zhu, S. W. Wang, J. Du, Q. Jin, T. R. Zhang, F. Y. Cheng, J. Chen, *Nano Lett.* **2014**, *14*, 153.
[12] Z. H. Wen, S. M. Cui, H. Kim, S. Mao, K. Yu, G. H. Lu, H. H. Pu, O. Mao, J. H. Chen, *J. Mater. Chem.* **2012**, *22*, 3300.
[13] D. Deng, J. Y. Lee, *J. Mater. Chem.* **2010**, *20*, 8045.
[14] J. Qin, C. N. He, N. Q. Zhao, Z. Y. Wang, C. S. Shi, E. Z. Liu, J. J. Li, *ACS Nano* **2014**, *8*, 1728.
[15] G. H. Zhang, J. Zhu, W. Zeng, S. C. Hou, F. L. Gong, F. Li, C. C. Li, H. G. Duan, *Nano Energy* **2014**, *9*, 61.

[16] X. Y. Li, Y. M. Chen, L. M. Zhou, Y. W. Mai, H. T. Huang, *J. Mater. Chem. A* **2014**, *2*, 3875.
[17] X. Y. Li, Y. M. Chen, H. M. Yao, X. Y. Zhou, J. Yang, H. T. Huang, Y. W. Mai, L. M. Zhou, *RSC Adv.* **2014**, *4*, 39906.
[18] Y. X. Tang, Y. Y. Zhang, J. Y. Deng, J. Q. Wei, H. L. Tam, B. K. Chandran, Z. L. Dong, Z. Chen, X. D. Chen, *Adv. Mater.* **2014**, *26*, 6111.
[19] H. G. Wang, D. L. Ma, X. L. Huang, Y. Huang, X. B. Zhang, *Sci. Rep.* **2012**, *2*, 701.
[20] G. Q. Zhang, H. B. Wu, T. Song, U. Paik, X. W. Lou, *Angew. Chem. Int. Ed.* **2014**, *53*, 1.
[21] Y. Y. Zhou, C. S. Jo, J. Lee, C. W. Lee, G. J. Qao, S. H. Yoon, *Microporous Mesoporous Mater.* **2012**, *151*, 172.
[22] J. Z. Chen, L. Yang, Z. X. Zhang, S. H. Fang, S. I. Hirano, *Chem. Commun.* **2013**, *49*, 2792.
[23] J. Y. Liao, A. Manthiram, *Adv. Energy Mater.* **2014**, *4*, 1400403.
[24] J. Y. Shin, J. H. Joo, D. Samuelis, J. Maier, *Chem. Mater.* **2011**, *24*, 543.
[25] X. Lu, G. Wang, T. Zhai, M. Yu, J. Gan, Y. Tong, Y. Li, *Nano Lett.* **2012**, *12*, 1690.
[26] M. Stefik, F. J. Heiligtag, M. Niederberger, M. Grätzel, *ACS Nano* **2013**, *7*, 8981.
[27] M. Kruk, M. Jaroniec, *Chem. Mater.* **2001**, *13*, 3169.
[28] J. H. Jeun, K. Y Park, D. H. Kim, W. S. Kim, H. C. Kim, B. S. Lee, H. G. Kim, W. R. Yu, K. Kang, S. H. Hong, *Nanoscale* **2013**, *5*, 8480.
[29] L. Wang, D. Wang, Z. H. Dong, F. X. Zhang, J. Jin, *Nano Lett.* **2013**, *13*, 1711.
[30] B. Zhang, Q. B. Zheng, Z. Huang, S. W. Oh, J. K. Kim, *Carbon* **2011**, *49*, 4524.
[31] X. Liu, H. Xu, L. R. Grabstanowicz, S. M. Gao, Z. Z. Lou, W. J. Wang, B. B. Huang, Y. Dai, T. Xu, *Catal. Today* **2014**, *225*, 80.
[32] Z. Liang, G. Zheng, W. Li, Z. W. Seh, H. Yao, K. Yan, D. Kong, Y. Cui, *ACS Nano* **2014**, *8*, 5249.
[33] L. Zhang, G. Q. Shi, *J. Phys. Chem. C* **2011**, *115*, 17206.
[34] T. Xu, W. Hou, X. Shen, H. Wu, X. Li, J. Wang, Z. Jiang, *J. Power Sources* **2011**, *196*, 4934.
[35] J. D. Zhuang, Q. F. Tian, H. Zhou, Q. Liu, P. Liu, H. M. Zhong, *J. Mater. Chem.* **2012**, *22*, 7036.
[36] X. R. Xia, N. A. Monteiro-Riviere, S. Mathur, X. F. Song, L. S. Xiao, S. J. Oldenberg, B. Fadeel, J. E. Riviere, *ACS Nano* **2011**, *5*, 9074.
[37] L. Qie, W. M. Chen, Z. H. Wang, Q. G. Shao, X. Li, L. X. Yuan, X. L. Hu, W. X. Zhang, Y. H. Huang, *Adv. Mater.* **2012**, *24*, 2047.
[38] B. Zhang, Y. Yu, Z. D. Huang, Y. B. He, D. H. Jang, W. S. Yoon, Y. W. Mai, F. Y. Kang, J. K. Kim, *Energy Environ. Sci.* **2012**, *5*, 9895.
[39] S. Q. Chen, P. Chen, M. H. Wu, D. Y. Pan, Y. Wang, *Electrochem. Commun.* **2010**, *12*, 1302.
[40] S. Q. Chen, Y. Wang, H. J. Ahn, G. X. Wang, *J. Power Sources* **2012**, *216*, 22.
[41] Y. M. Chen, X. Y. Li, X. Y. Zhou, H. M. Yao, H. T. Huang, Y. W. Mai, L. M. Zhou, *Energy Environ. Sci.* **2014**, *7*, 2689.
[42] Y. M. Chen, Z. G , Lu, L. M. Zhou, Y. W. Mai, H. T. Huang, *Nanoscale* **2012**, *4*, 6800.